JBIC Journal of Biological Inorganic Chemistry
https://doi.org/10.1007/s00775-019-01688-9

ORIGINAL PAPER

A novel series of mixed-ligand M(II) complexes containing 2,2′-bipyridyl as potent α-glucosidase inhibitor: synthesis, crystal structure, DFT calculations, and molecular docking

Davut Avcı[1] · Sümeyye Altürk[1] · Fatih Sönmez[2] · Ömer Tamer[1] · Adil Başoğlu[1] · Yusuf Atalay[1] · Belma Zengin Kurt[3] · Necmi Dege[4]

Received: 11 May 2019 / Accepted: 10 July 2019

Abstract

Diabetes mellitus (DM) is a common degenerative disease and characterized by high blood glucose levels. Since the effective antidiabetic treatments attempt to decrease blood glucose levels, keeping glucose under control is very important. Recent studies have demonstrated that α-glucosidase inhibitor improves postprandial hyperglycemia and then reduces the risk of developing type 2 diabetes in patients. Therefore, the design and synthesis of high affinity glucosidase inhibitors are of great importance. In this regard, novel series of mixed-ligand M(II) complexes containing 2,2′-bipyridyl {[$Hg(6\text{-mpa})_2(bpy)(OAc)]\cdot 2H_2O$, (**1**), $[Co(6\text{-mpa})_2(bpy)_2]$, (**2**), $[Cu(6\text{-mpa})(bpy)(NO_3)]\cdot 3H_2O$, (**3**), $[Mn(6\text{-mpa})(bpy)(H_2O)_2]$, (**4**), $[Ni(6\text{-mpa})(bpy)(H_2O)_2]\cdot H_2O$, (**5**), $[Fe(6\text{-mpa})(bpy)(H_2O)_2]\cdot 2H_2O$, (**6**), $[Fe(3\text{-mpa})(bpy)(H_2O)_2]\cdot H_2O$, (**7**)} were synthesized as potential α-glucosidase inhibitors. Their effects on α-glucosidase activity were evaluated. All synthesized complexes displayed α-glucosidase inhibitory activity with IC_{50} values ranging from 0.184 ± 0.015 to > 600 μM. The experimental spectral analyses were carried out using FT–IR and UV–Vis spectroscopic techniques for these complexes characterized by XRD and LC–MS/MS. Moreover, the calculations at density functional theory approximation were used to obtain optimal molecular geometries, vibrational wavenumbers, electronic spectral behaviors, and major contributions to the electronic transitions for the complexes **1**–**7**. Finally, to display interactions between the synthesized complexes and target protein (the template structure *Saccharomyces cerevisiae* isomaltase), the molecular docking study was carried out.

Keywords 2,2′-Bipyridyl and 6-methylpyridine-2-carboxylic acid · XRD, FT-IR and UV–Vis · α-Glucosidase · Docking · DFT/HSE06

Abbreviations

FMO	Frontier molecular orbital
HSE06	Heyd–Scuseria–Ernzerhof (HSE) exchange with Perdew–Burke–Ernzerhof (PBE) correlation functional (known as HSEh1PBE)
IC_{50}	Half-maximal (50%) inhibitory concentration
LO/NLO	Linear/nonlinear optics
MEP	Molecular electrostatic potential
MTT	3-(4,5-Dimethyl-2-thiazolyl)-2,5-diphenyl-2H-tetrazolium bromide
NBO	Natural bond orbital
PCM	Polarizable continuum model
T2DM	Type 2 diabetes mellitus
TD/DFT	Time-dependent density functional theory

Electronic supplementary material The online version of this article (https://doi.org/10.1007/s00775-019-01688-9) contains supplementary material, which is available to authorized users.

✉ Davut Avcı
davci@sakarya.edu.tr

[1] Department of Physics, Faculty of Arts and Sciences, Sakarya University, 54187 Sakarya, Turkey

[2] Pamukova Vocational School, Sakarya University of Applied Sciences, 54055 Sakarya, Turkey

[3] Department of Pharmaceutical Chemistry, Faculty of Pharmacy, Bezmialem Vakif University, 34093 Istanbul, Turkey

[4] Department of Physics, Faculty of Arts and Sciences, Ondokuz Mayıs University, 55139 Samsun, Turkey

Published online: 17 July 2019

Introduction

Diabetes mellitus (DM), characterized by high blood glucose levels, is one of the most common metabolic degenerative diseases in the world [1, 2]. The most common cause of type 2 diabetes is insulin resistance. The prevalence of T2DM in all age groups in the world is increasing and it is estimated that it will reach from 2.8% in 2000 to 4.4% in 2030 [3]. Many antidiabetic treatments focus on lowering blood glucose levels; therefore, glucose control is an effective treatment for diabetes. To release glucose, it is well known that α-glucosidase (EC 3.2.1.20) which is a carbohydrate hydrolase specifically hydrolyses the 1,4-α-glucopyranosidic bond [4]. α-Glucosidase, which is catalyzes the cleavage of absorbable monosaccharides, beginning from disaccharides and oligosaccharides, is a critical enzyme for the digestion of carbohydrates [5]. The missions of α-glucosidase for mammals include intestinal digestion of dietary carbohydrates, glycoprotein folding and maturation, and glycogen degradation. Moreover, the inhibition of α-glucosidases and related enzymes plays an important role in the treatment of diabetes, cancer, human immunodeficiency virus (HIV/AIDS), and other degenerative diseases [6, 7].

α-Glucosidase inhibitors (AGIs) delay the digestion of carbohydrates and prolong the digestion time in general carbohydrates, slows the absorption of glucose and thus blunt the increase of postprandial plasma glucose. Inhibitors reducing postprandial hyperglycemia have an important role in the treatment of T2DM and pre-diabetes situations. Recent studies have shown that α-glucosidase inhibitor improves postprandial hyperglycemia and subsequently reduces the risk of developing type 2 diabetes in patients with impaired glucose resistance [8–10]. Several X-ray crystallographic studies on complexes with substrates and inhibitors have revealed that the inhibition of glucosidases can occur with enzymic hydrolysis of glucosidases. This inhibition involves a two-step mechanism in which a covalent glycosyl-enzyme intermediate is formed and hydrolyzed via oxocarbenium ion like transition states [11–13]. Various AGIs such as acarbose, voglibose, and miglitol molecules are clinically used to treat T2DM [14]. Besides, a few AGIs commercially available in pharmacies and they do not meet their needs due to the side effects. Therefore, the design and synthesis of high affinity glucosidase inhibitors are of great importance. In this direction, the healing effects of complexes containing different metal ions on individuals with Type 2 diabetes have been subject of intensive research. Particularly, metal complexes of nitrogen-containing ligands are frequently used in the field of coordination chemistry due to structurally, spectroscopically and catalytically similar to some enzyme–substrate complexes in our body [3, 15–18].

The synthesis and physicochemical properties of pyridine derivatives, such as picolinic acid, are important for the synthesis of different structures including coordination complexes, due to their different potential applications in catalysis, nonlinear optics, luminescence, ion exchange, and material chemistry [19–21]. The ligands bearing conjugated electron-rich heteroaromatic rings, such as 2,2′-bipyridyl, 1,10-phenanthroline, etc., are important in the understanding of electron transfer processes, mixed valence complexes, photochemistry. They are also used for the formation of different metal complexes including transition metals in biological processes [22–24]. Wang et al. investigated the inhibition activity against α-glucosidase of various metal ions, such as Cu^{2+}, Zn^{2+}, V^{4+}, Ni^{2+}, Fe^{2+}, Mn^{2+}, etc. [25]. Up until now, the different studies containing metal ion on the insulin-like stimulation of glucose oxidation in rat adipocytes with vanadyl (IV) ions [26], insulin-like effect of zinc on adipocytes [27], copper complexes presenting a physiological approach in the treatment of chronic diseases [28], and the increasing of chromium uptake for improve glucose and insulin variables in individuals with type 2 diabetes [29] have been reported. In addition, insulinomimetic activity studies for release of free fatty acid (FFA) from rat adipocytes, different metal complexes including picolinic acid, and its derivatives have been performed for $VO(pa)_2$ [30], $VO(6mpa)_2$, $VO(3\text{-}mpa)_2$ [30], $Cr(pa)_3$, $Mn(pa)_2$, $Mn(pa)_3$, $Fe(pa)_2$, $Fe(pa)_3$, $Co(pa)_2$, $Ni(pa)_2$, $Cu(pa)_2$ [31] and $Zn(pa)_2$, $Zn(3\text{-}mpa)_2$, $Zn(6\text{-}mpa)_2$ [32]. Finally, the IC_{50} values of the various metal complexes including picolinate (pa) and its derivatives for alpha-glucosidase enzyme activity have been obtained for $Cu(pa)_2$, $Zn(pa)_2$, $VO(pa)_2$ [33], and $Zn(6mpa{-}ma)_2SO_4$ [34]. As far as we know, there are no α-glucosidase enzyme activity studies of the mixed-ligand metal complexes including 6-mpa ligand except for 6-mpa with thiocyanate/4(5)methylimidazole (4(5)MeI) in the literature [7, 35].

As a result of our ongoing works, novel metal(II) complexes (complexes **1**–**7**) containing 6-methylpyridine-2-carboxylic acid/3-methylpyridine-2-carboxylic acid (6-mpa/3-mpa) and 2,2′-bipyridyl (bpy) were synthesized for the first time. The crystal structures of Hg(II) and Co(II) complexes were determined by XRD spectroscopic technique and molecular structures of Cu(II), Mn(II), Ni(II), and Fe(II) complexes were defined by mass spectrometry (MS). The α-glucosidase enzyme inhibition and electronic spectral behavior studies were experimentally investigated. Furthermore, the structural, spectral, electronic, second-, and third-order nonlinear optical parameters of complexes **1**–**7** in gas phase and ethanol solvent were examined using DFT/HSE06/6-311G(d,p)/LanL2DZ level. After all, to determine the ligand protein interactions, molecular-docking study was fulfilled.

Experimental and computational details

Physical measurements

FT-IR spectra of the novel synthesized complexes were recorded using a Perkin Elmer Spectrum-Two FT-IR spectrophotometer equipped with Perkin Elmer UATR-TWO diamond ATR. To examine the UV–Vis electronic absorption spectra of the complexes **1**–**7** in the range of 900–200 nm, a HITACHI U-2900 UV/VIS spectrophotometer in ethanol solvent with quartz cell of 1 cm was used. Mass spectra were obtained with SHIMADZU-8030 or AGILENT-6460 LC−MS/MS quadrupole mass spectrometer, equipped with an electrospray ionization (ESI +/−) used in MS/MS mode.

X-ray structure determination

A Stoe IPDS II diffractometer using Mo–Kα ($\lambda = 0.71073$ Å) radiation at 296 K for data collection was applied to suitable single crystals of the complexes **1**, **2**. The crystal structure determine details are given in Table 1. The crystal structures were solved by direct methods using SHELXT [36] and refined by full-matrix least-squares methods on F2 using SHELXL-97 [36]. The hydrogen atoms bonding to carbon atoms were located from different maps and then treated as riding atoms with C–H distances of 0.96 Å. The H atoms of water were located in a difference map refined freely. Molecular diagrams were created using MERCURY [37]. Supramolecular analyses were made and the diagrams were prepared with the aid of PLATON [38].

Table 1 Crystal data and structure refinement parameters for the complexes **1** and **2**

	Complex **1**	Complex **2**
Empirical formula	$C_{19}H_{21}HgN_3O_6$	$C_{24}H_{20}CoN_4O_4$
Formula weight	587.98	487.37
Crystal system	Monoclinic	Orthohombic
Space group	$P2_1/c$	Pbca
Temperature	296	296
Radiation type	Mo *K*α	Mo *K*α
Wavelength	0.71073	0.71073
Crystal size (mm)	0.71×0.62×0.55	0.78×0.75×0.59
a (Å)	9.178 (4)	13.2756 (6)
b (Å)	21.630 (9)	19.049 (1)
c (Å)	10.742 (4)	17.2348 (11)
α (°)	90	90
β (°)	107.64 (3)	90
γ (°)	90	90
V (Å^3)	2032.04 (15)	4358.5 (4)
Z	4	8
F(000)	1136	2008
Density (g cm^{-3})	1.922	1.485
μ (mm^{-1})	7.62	0.83
θ range (°)	1.9–27.8	1.9–30.0
Measured refls.	14504	16570
Independent refls.	3990	4292
R_{int}	0.051	0.081
S	0.96	1.00
R1/wR2	0.028/0.060	0.045/0.108
Max/min (eÅ^{-3})	0.49/− 1.07	0.85/− 0.54

Materials and synthesis of the complexes 1–7 {[Hg(6-mpa)$_2$(bpy)(OAc)]·2H$_2$O, (1), [Co(6-mpa)$_2$(bpy)$_2$], (2), [Cu(6-mpa)(bpy)(NO$_3$)]·3H$_2$O, (3), [Mn(6-mpa)(bpy)(H$_2$O)$_2$], (4), [Ni(6-mpa)(bpy)(H$_2$O)$_2$]·H$_2$O, (5), [Fe(6-mpa)(bpy)(H$_2$O)$_2$]·2H$_2$O, (6), [Fe(3-mpa)(bpy)(H$_2$O)$_2$]·H$_2$O, (7)}

All of the chemical reagents used in this study are analytical grade commercial products. 6-mpaH (6-methylpyridine-2-carboxylic acid), 3-mpaH (3-methylpyridine-2-carboxylic acid) and 2,2′-bipyridyl (bpy), mercury(II) acetate ($Hg(OAc)_2$), cobalt(II) acetate tetrahydrate ($Co(OAc)_2{\cdot}4H_2O$), copper(II) nitrate trihydrate ($Cu(NO_3)_2{\cdot}3H_2O$), manganese(II) acetate tetrahydrate ($Mn(OAc)_2{\cdot}4H_2O$), nickel(II) chloride ($NiCl_2$) and iron(II) chloride ($FeCl_2$) were purchased from Sigma-Aldrich. The synthesis methods of the complexes **1**–**7** are as follows (see Scheme 1).

Synthesis of the complex **1**: the 6-methylpyridine-2-carboxylic acid (1 mmol) and 2,2′-bipyridyl (1 mmol) was separately dissolved in acetonitrile solution (10 ml). Then, two mixture slowly added to an acetonitrile solution (10 ml) of mercury(II) acetate (1 mmol) at the same time. The last mixture was stirred for 6 h, and evaporated for a week at room temperature. At the end of this process, the formed crystals for complex **1** were filtered off, washed thoroughly with distilled water, and finally air-dried at room temperature. The single-crystal structure for the complex **1** was obtained as colorless in stick shaped.

Synthesis of the complexes **2**, **3**: the solid 6-methylpyridine-2-carboxylic acid (2/1 mmol for complex **2/3**), 2,2′-bipyridyl (1 mmol) and cobalt(II) acetate tetrahydrate (1 mmol)/copper (II) acetate (1 mmol) (for complex **2/3**) were added to a mixture of ethanol and water (20 ml, 1:1) under continuous stirring. The obtained solution was stirred at 60 °C for 3 h, and evaporated for 15 days at room temperature. At the end of this process, the formed crystals for complex **2** and powder product for complex **3** were filtered off, washed thoroughly with distilled water, and finally air-dried at room temperature. The single crystals of the complex **2** were obtained as red in prism

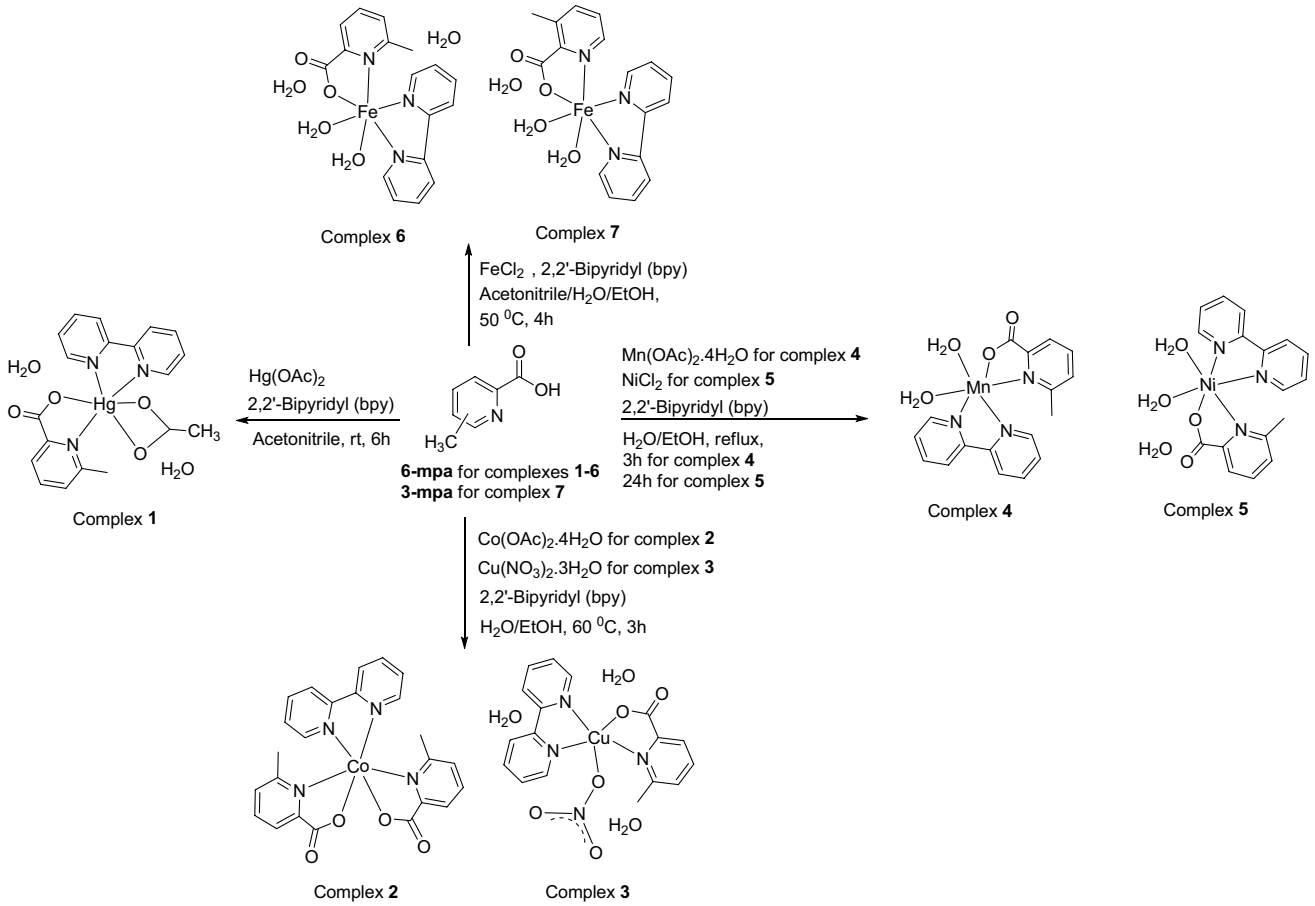

Scheme 1 The synthesis of the complexes **1**–**7**

shaped. Anal. Calc. for $C_{17}H_{20}N_4O_8Cu$ (complex **3**): C, 43.27; H, 4.27; N, 11.87. Exact mass (*m*/*z*): 471.06. Found: ESI–LC–MS/MS (*m*/*z*): 471 ($[M]^+$). The mass spectrum for complex **3** is given in Fig. S1.

Synthesis of the complexes **4**, **5**: the solid 6-methylpyridine-2-carboxylic acid (1 mmol), 2,2′-bipyridyl (1/2 mmol for complex **4/5**) and manganese(II) acetate tetrahydrate (1 mmol)/nickel(II) chloride (1 mmol) (for complex **4/5**) were added to a mixture of ethanol and water (20 ml, 1:1) under continuous stirring at 70 °C. After the last mixture was refluxed for 4 h, it was allowed to evaporate at room temperature. After the period of 15 days, the powder products for complexes **4**, **5** were filtered off, washed thoroughly with distilled water, and finally air-dried at room temperature. Anal. Calc. for $C_{17}H_{18}N_3O_4Mn$ (complex **4**): C, 53.27; H, 4.73; N, 10.96. Exact mass (*m*/*z*): 383.07. Found: ESI–LC–MS/MS (*m*/*z*): 387 ($[M+4H]^+$). Anal. Calc. for $C_{17}H_{20}N_3O_5Ni$ (complex **5**): C, 50.41; H, 4.98; N, 10.37. Exact mass (*m*/*z*): 404.08. Found: ESI–LC–MS/MS (*m*/*z*): 405 ($[M]^+$). The mass spectra for complexes **4**, **5** are given in Figs. S2 and S3.

Synthesis of the complexes **6**, **7**: the solid 6-methylpyridine-2-carboxylic acid (1 mmol for complex **6**), 3-methylpyridine-2-carboxylic acid (1 mmol for complex **7**), 2,2′-bipyridyl (1 mmol) and iron(II) chloride (1 mmol) were added to a mixture of acetonitrile, ethanol, and water (20 ml, 2:2:1) under continuous stirring at 50 °C. The last mixture was stirred within closed vial at 50 °C for 4 h and evaporated for 15 days at room temperature. At the end of this process, the powder products for complexes **6**, **7** were filtered off, washed thoroughly with distilled water, and finally air-dried at room temperature. Anal. Calc. for $C_{17}H_{22}N_3O_6Fe$ (complex **6**): C, 48.59; H, 5.28; N, 10.00. Exact mass (*m*/*z*): 459.05. Found: ESI–LC–MS/MS (*m*/*z*): 461.3 ($[M+K]^+$). Anal. Calc. for $C_{17}H_{20}N_3O_5Fe$ (complex **7**): C, 50.77; H, 5.01; N, 10.45. Exact mass (*m*/*z*): 402.08. Found: ESI–LC–MS/MS (*m*/*z*): 403 ($[M]^+$). The mass spectra for complexes **6**, **7** are given in Figs. S4 and S5.

α-Glucosidase inhibition assay

α-Glucosidase inhibition activities of the synthesized complexes (**1**–**7**) were determined by doing small changes on Sun's protocol [39]. The α-glucosidase from *Saccharomyces cerevisiae* (Sigma, G5003) was determined as the target protein using *p*-nitrophenyl-α-D-glucopyranoside (pNGP, Sigma, N1377) as the substrate. The compounds and genistein were dissolved in DMSO. The enzyme and the substrate were dissolved in potassium phosphate buffer (0.05 M, pH 6.8). The enzymatic reaction mixture composed of α-glucosidase (0.02 U, 20 µl), substrate (1.25 mM, 30 µl), test compounds (10 µl), and potassium phosphate buffer (140 µl) was incubated at 37 °C for 30 min. After 30 min of incubation, the absorbance of yellow color produced due to the formation of *p*-nitrophenol was measured using Synergy H1 (BioTek, USA) 96-well microplate reader at 405 nm. All experiments were performed in triplicates. The surveying of α-glucosidase inhibition activity for the complexes **1**–**7** was fulfilled on the basis of our previously reported study [7]:

$$\text{Glucosidase inhibition} = \left[\left(A_c - A_s\right)/A_c\right] \times 100,$$

where A_c is the absorbance of control and A_s is the absorbance of samples, respectively. The calculation of IC_{50} values was performed using Graphpad Software.

Cytotoxicity of the complex **1** was tested according to our previous study [40].

Computational procedure

To investigate quantum chemical calculations of the synthesized complexes (**1**–**7**), GAUSSIAN 09, Revision D01, [41] and GaussView 5 program [42] were used. To obtain the reasonable results for the ground-state geometries and vibrational wavenumbers of the complexes **2**–**7**, the DFT/HSE06 hybrid density functional [43, 44] and the combined basis set of 6-311G(d,p) [45] for C, N, O, H atoms, and LanL2DZ [46] for Co, Cu, Mn, Ni, and Fe atoms was selected. The same parameters for complex **1** were obtained using DFT/HSE06/LanL2DZ level. To examine the electronic spectral parameters of complexes **1**–**7** in ethanol solvent and gas phase, the time-dependent DFT (TD-DFT) level [47] with conductor-like polarizable continuum model (CPCM) [43] was applied. Frontier molecular orbital (FMO) energies and related parameters were obtained at the same level. To define coordination environment around the metal ion centers and hydrogen-bonding interaction, natural bond orbital (NBO) analysis [48] was carried out. The microscopic linear polarizability (α and $\Delta\alpha$), second- and third-order nonlinear optical parameters (β and γ) in gas phase and ethanol solvent were computed at the same level and basis set. Finally, the molecular electrostatic potential (MEP) surfaces were surveyed using the same method.

Docking procedure

To investigate protein–ligand interactions between the synthesized complexes (**1**–**7**) and target protein (the template structure *S. cerevisiae* isomaltase) used as rigid, we performed the molecular-docking study using the iGEMDOCK program [49]. The ligand structures were selected as the ground-state energy conformations of each synthesized complexes obtained by GAUSSIAN program. GEMDOCK parameters in the flexible docking were applied as the initial step sizes ($\sigma = 0.8$ and $\psi = 0.2$; step-size vectors of decreasing-based Gaussian mutation and self-adaptive Cauchy mutation, respectively), family competition length ($L = 2$), population size ($N = 800$), and recombination probability ($p_c = 0.3$). For each ligand screened, when the convergence falls below a certain threshold or reaches a maximum preset value of 80, GEMDOCK was set to stop optimization. Thus, GEMDOCK provided 800 solutions in one generation and terminated after it finished 64,000 solutions for each docked ligand.

Results and discussion

Analysis of molecular geometries of the synthesized complexes (1–7)

Scheme 1 displays the synthesis procedures for complexes **1**–**7**. The single-crystal structures of complexes **1**, **2** were determined by X-ray diffraction analysis. Table 1 depicts the crystal data and structure refinement parameters of complexes **1**, **2**. The space groups of complexes **1**, **2** are found as $P2_1/c$ and Pbca, respectively. Figures 1 and S6 show the crystal and optimized theoretical molecular structures of the complexes **1**–**7**. The coordination around M(II) atom in complexes **1**, **2**, **4**–**7** is similarly described as a distorted octahedron geometry, while the coordination around Cu(II) atom in complex **3** is determined as a distorted trigonal bipyramidal geometry. The complexes **4**–**6** consist of Mn(II), Ni(II), and Hg(II) central ions coordinated by 6-mpa, bpy, and two water ligands, respectively, while the complex **1** includes a Hg(II) ion coordinated by 6-mpa, bpy, and an acetate (OAc) ligands. The complex **2** contains a central Co(II) ion coordinated by two 6-mpa and bpy ligands, whereas the complex **3** includes a central Cu(II) ion coordinated by 6-mpa, bpy, and nitrate ligands, and three water molecules. As for the complex **7**, the coordination around of the central Fe(II) ion is constituted by 3-mpa, bpy, and two water ligands.

By considering experimental and theoretical results of complexes **1**, **2**, the N, O atoms of pyridine and carboxylate

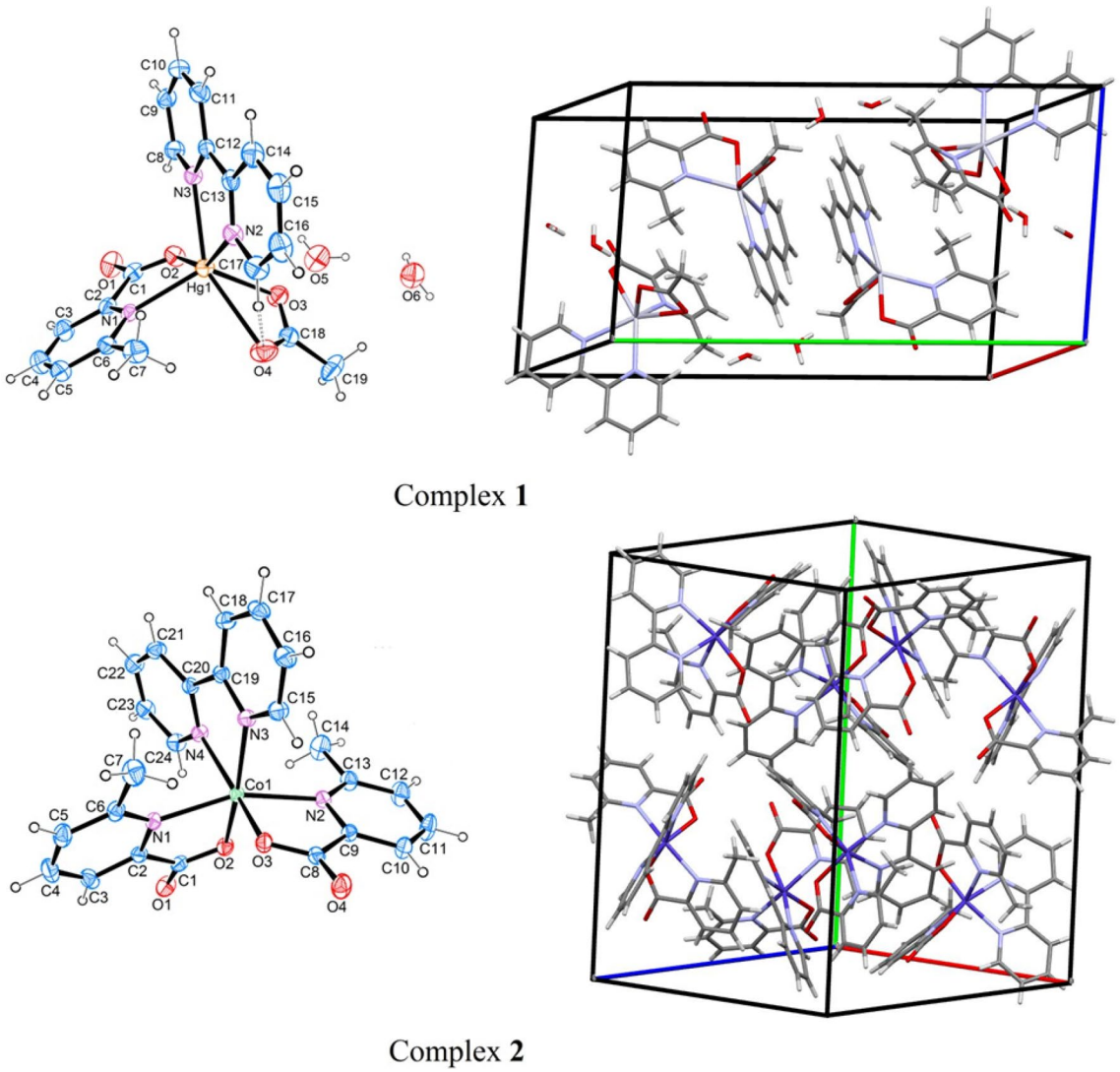

Fig. 1 Single crystal and packing structures for complexes **1** and **2**

parts constitute the five-membered chelate rings formed by coordinating to the centers of Hg(II) and Co(II). Similarly, this ring consists of coordination of the N atoms of bpy ligands to Hg(II) and Co(II) centers, as can be seen in Fig. 1. The M(II)-N1/N2/N3/N4 and M(II)-O2/O3 bond lengths for complexes **1**, **2** have been observed at the range of 2.144(2)–2.393(4) and 2.023(19)–2.349(4) Å, respectively. These distances have been calculated at the range of 1.932–2.492 and 1.905–2.311 Å by HSE06 level. These results are consistent with the same bond lengths in previous by reported Mpa/6-mpa complexes [7, 50–54]. The same bond lengths of the complexes **3**–**7** are presented as only theoretical results (see Table S1). Considering the coordination of M(II) center with N atoms of bpy, the Hg/Co/Cu/Mn/Ni/Fe–N bond distances change by depending on the coordination around M(II). The O–M–N and N–M–N bond angles belonging to five-membered chelate ring formed by metal(II) ion and coordinated O and N atoms of 6-mpa ligand and two N atoms of bpy ligand are obtained at the range of 71.5°–81.7° and 66.5°–83.0° by HSE06 level, respectively (see Table S1). The bond lengths and angles belonging to the coordination geometry around M(II) atom for complexes **1**–**7** are consistent with previously reported values of different complex structures [7].

Figure 1 demonstrates the crystal-packing structures of complexes **1**, **2** determined by C–H···O-type intermolecular hydrogen-bonding interactions between the carboxylate group of 6-mpa ligand and –CH group of bpy ligand. The other O–H···O hydrogen bond interactions occur between uncoordinated O–H bond of two waters and O3/O5 atoms of acetate/water ligand. All possible interactions for the complexes **1**, **2** together with symmetry codes are presented in Table 2.

Table 2 Hydrogen–bond parameters for the complexes **1** and **2** (Å and °)

D–H···A	D–H	H···A	D···A	D–H···A
Complex **1**				
C8–H8···O2	0.93	2.43	3.078 (7)	127
C17–H17···O4	0.93	2.50	3.175 (8)	129
C16–H16···O1^{i}	0.93	2.37	3.111 (7)	136
O6–H6A···O1^{ii}	0.82 (2)	2.10 (4)	2.884 (7)	161 (9)
O6–H6B···O5	0.83 (2)	2.02 (4)	2.753 (9)	147 (8)
O5–H5A···O3	0.81 (2)	2.00 (3)	2.789 (6)	165 (9)
O5–H5B···O5^{ii}	0.80 (2)	2.32 (6)	2.747 (13)	114 (6)
Complex **2**				
C18–H18···O1^{i}	0.93	2.63	3.364 (4)	137
C16–H16···O1^{ii}	0.93	2.48	3.363 (4)	159
C23–H23···O4^{iii}	0.93	2.56	3.441 (4)	158
C15–H15···O3	0.93	2.64	3.171 (4)	117
C24–H24···O2	0.93	2.63	3.151 (4)	116
C5–H5···O1^{iv}	0.93	2.59	3.159 (4)	120

Symmetry codes: complex **1** (i) $x+1, y, z+1$; (ii) $-x+1, -y+1, -z$. Complex **2** (i) $x-1/2, -y+3/2, -z+1$; (ii) $-x+1/2, y-1/2, z$; (iii) $x, -y+3/2, z+1/2$; (iv) $x-1/2, y, -z+1/2$

Analysis of vibrational frequency

To assign vibrational modes and determine coordination environment around the M(II) for complexes 1–**7**, we have investigated the FT–IR spectra and theoretical IR spectra for the complexes 1–**7**. Theoretical results obtained by HSE06/6-311G(d,p)/LanL2DZ level and scaled by 0.96 [55] are given in Table 3. Figure 2a, b depicts the FT–IR spectra of the complexes **1**–**7** at the range of 4000–400 and 1750–400 cm^{-1}. It was reported that the stretching vibration of OH group approximately appears at 3700–3500 cm^{-1} range [56]. The OH stretching vibration modes of water ligands in complexes **1**, **3**–**7** were observed at the range of 3401–3110 cm^{-1}, the corresponding modes were calculated at 3242–3411 cm^{-1} range (see Table 3). It is well known that the CH stretching vibrations of the aromatic and aliphatic molecules emerge at above 3000 and below 3000 cm^{-1}, respectively [56]. The ring CH stretching vibration modes of 6-mpa/3-mpa and bpy ligands were appeared at above 3000 cm^{-1}, as can be shown in FT–IR of the complexes **1**–**7** (see Table 3). The other important vibrational mode belonging to coordinated or uncoordinated water ligands, the scissoring peaks were emerged at 1491–1663 cm^{-1} range, and these modes were found to be 1635–1639 cm^{-1} range by HSE06/6-311G(d,p)/LanL2DZ level. These results exhibit that there are good agreement between experimental and theoretical vibrational wavenumbers. The CH in-plane bending peaks of 6-mpa and 3-mpa ligands arisen approximately at 1400 cm^{-1} are consistent with previously reported results [7, 40].

In the complexes **1**–**7**, the asymmetric and symmetric COO^{-} stretching vibration modes play an important role on the formation of five-membered chelate ring, constituted by the coordination environment of M(II) ions. As can be seen in Fig. 2b, the asymmetric/symmetric COO^{-} stretching modes from FT-IR spectra of complexes **1**–**7** were found to be 1591/1313, 1630/1313, 1627/1316, 1640/1250, 1639/1374, 1620/1342, and 1601/1320 cm^{-1}. The experimental/theoretical difference between the symmetric and asymmetric COO^{-} stretching modes was found to be 390–278/417–300 cm^{-1} range display that 6-mpa and 3-mpa ligand coordinates to metal ions as a monodentate ligand via carboxylate group. These results are coherent with different metal complexes [7, 40, 51–53, 57]. In complex **3**, the NO-stretching mode of nitrate ligand experimentally and theoretically appears at 1497/1595 cm^{-1} (see Table 3), and this mode is consistent with results of reported different metal complex structures [58, 59]. The other detailed vibrational modes belonging 6-mpa, 3-mpa, bpy, acetate, nitrate, and water ligands were assigned in Table 3.

Analyses of electronic absorption spectra, FMOs, MEP, and NBO parameters

To interpret the electronic absorption spectra, major electronic transitions, oscillator strengths were investigated using TD–HSE06 method with 6–311G(d,p)/LanL2DZ basis sets. Figure 3 demonstrates the UV–Vis spectra of the complexes **1**–**6** in ethanol solvent. The remarkable contributions from FMOs to the electronic transitions were described using SWizard [60] program. The electronic spectral parameters are comparatively given in Table S2. Theoretical absorption peak corresponding to the highest electronic absorption wavelength in ethanol solvent was appointed as d → d originated from metal to metal charge transfer (MMCT), metal to ligand, and ligand to metal charge transfer (MLCT) transitions (see Table S2). This peak for complexes **2**–**7** in ethanol solvent was calculated at 560, 594, 568, 596, 535, and 549 nm with the contributions H → Lα(87%), H − 25 → L + 1 β (+ 12%)/H − 25 → L β (+ 8%), H − 2 → L + 7 (+ 43%)/H − 1 → L (+ 9%), H − 3 → L + 1 β (+ 23%)/H − 4 → L + 5 β (+ 14%), H − 2 → L + 4 α (+ 23%)/H − 3 → L + 4 β (+ 23%), and H − 1 → L α (+ 38%)/H → L β (+ 34%), respectively. The corresponding experimental peaks for complexes **5**, **6** in ethanol solvent were observed at 521 and 522 nm, as can be seen in Fig. 3. The absorption peaks of the complexes **1**–**7** in ethanol solvent arisen from n → π* and π → π* transitions between metal–ligand and ligand–ligand charge transfers were emerged at the range of 276–217, 372–220, 310–211, 277–204, 306–213, 346–244, and 339–205 nm. The corresponding theoretical peaks in ethanol solvent were found to be 277–252, 376–296, 329–251, 284–228, 315–245,

Table 3 Comparison of the FT–IR and calculated vibration frequencies for the complexes **1**–**7**

Assignments	Complex **1**		Complex **2**		Complex **3**		Complex **4**		Complex **5**		Complex **6**		Complex **7**	
	FT–IR	HSEh1PBE[a]	FT–IR	HSEh1PBE[a]	FT–IR	HSEh1PBE[a]	FT–IR	HSEh1PBE[a]	FT–IR	HSEh1PBE[a]	FT–IR	HSEh1PBE[a]	FT–IR	HSEh1PBE[a]
υ OH	3370	3732	–	–	3411	3735	3253	3735	3355	3770	–	3724	–	3711
υ OH	3242	3707	–	–	3253	3516	–	3629	–	3763	3366	3603	3410	3623
υ CH bpy	3105	3152	3106	3105	3086	3111	3054	3096	3094	3101	3073	3104	–	3102
υ CH mpa	–	3136	3192	3110	3114	3114	3086	3103	3075	3092	–	3095	3081	3090
υ CH_3 mpa	3071	3061	2990	3021	2991	3026	2991	3024	2910	2940	3025	3035	–	3022
υ CH_3 OAc	3028	3020	–	–	–	–	–	–	–	–	–	–	–	–
β HOH	1634	1630	–	–	1601	1635	1491	1575	1599	1627	1655	1639	1663	1637
υ COO^-	1591	1607	1630	1716	1627	1680	1640	1713	1639	1696	1620	1726	1601	1716
υ CC bpy	–	1595		1604		1616		1586	1472	1572	1569	1571		1572
υ CC mpa	–	1585	1595	1599	1519	1599	1586	1597	1568	1603	–	1570	1585	1582
υ NC mpa	–	1584	1249	1274	1474	1579	1177	1265	1284	1275	–	1264	1270	1270
υ NO	–	–	–	–	1497	1595	–	–	–	–	–	–	–	–
υ NC bpy	1577	1573		1299	–	1583	–	1280	1315	1303	1282	1296	1318	1297
β HCH OAc	–	1500	–	–	–	–	–	–	–	–	–	–	–	–
β HCH mpa	1488	1481	1403	1418	–	1416	1399	1426		1414	1426	1426		1433
β HCC bpy	1439	1452		1428	–	1455		1439		1438	1440	1440	1418	1406
β HCC mpa		1452	1443	1435	1440	1447	1440	1447	1443	1455		1448	1394	1391
υ COO^-	1313	1307	1313	1328	1316	1358	1250	1296	1374	1345	1342	1325	1320	1307
υ NO	–	–	–	–	–	1318	–	–	–	–	–	–	–	–
β OHO	–	–	–	–	–	–	–	–	–	997	806	819	769	783
γ HCCC bpy	1044	1040		991		998	910	945	976	965		946		937
γ HCCC mpa	1013	1019	1010	984	971	988		969	910	947	915	912	901	917
γ OOON	–	–	–	–	796	813	–	–	–	–	–	–	–	–
β OCO	650	652	799	798	765	801	771	782	–	794	–	–	–	–
β ONO	–	–	–	–	730	745	–	–	–	–	–	–	–	–
β HOFe	–	–	–	–	–	–			–	–	662	665	634	638
γ HOMnO	–	–	–	–	–	–	673	684	–	–	–	–	–	–
γ HOFeO	–	–	–	–	–	–			–	–	588	594	578	588
β HOMn	–	–	–	–	–	–	533	560	–	–	–	–	–	–
γ CoCCN	–	–	474	462	–	–	–	–	–	–	–	–	–	–
γ HOHO	–	–	–	–	–	–	–	–	469	458	–	–	–	–
γ OHOFe	–	–	–	–	–	–	–	–	–	–	422	425	432	441
β CNCu	–	–	–	–	432	442	–	–	–	–	–	–	–	–
γ CCuCN	–	–	–	–	–	426	–	–	–	–	–	–	–	–

Table 3 (continued)

Assignments	Complex **1**		Complex **2**		Complex **3**		Complex **4**		Complex **5**		Complex **6**		Complex **7**	
	FT–IR	HSEh1PBE[a]	FT–IR	HSEh1PBE[a]	FT–IR	HSEh1PBE[a]	FT–IR	HSEh1PBE[a]	FT–IR	HSEh1PBE[a]	FT–IR	HSEh1PBE[a]	FT–IR	HSEh1PBE[a]
υ MnN	–	–	–	–	–	–	413	403	–	–	–	–	–	–
γ CNiCN	–	–	–	–	–	–	–	–	416	390	–	–	–	–

υ, Stretching; β, in-plane bending; γ, out-of plane bending

[a]Scaled frequencies are in unit of cm^{-1}

341–300, and 340–303 nm range. It is detailed given in Table S2 that the remarkable contributions for electronic transitions risen from different frontier molecular orbitals. It is clear from Fig. 4 that the low absorption values of complexes **1**–**7** were attributed to intraligand charge transfer (ILCT).

Based on the Tauc and Menth's equation [52, 61], the optical bandgap energy values are obtained using the following equation:

$$(\alpha h\nu) = C(h\nu - E_g)^{1/2}, \quad (1)$$

where the absorption coefficient α is calculated by $\alpha = 2.303A/d$ formula [A is the absorbance in the UV–Vis region and d is the width of the cuvette (1 cm)], C is a proportionality constant related to the effective masses associated with the bands, $h\nu$ is the photon energy, and E_g is the direct optical bandgap energy. The E_g value is calculated by extrapolating the linear portion of the plot of $(\alpha h\nu)^2$ versus $(h\nu)$ to $(\alpha h\nu)^2 = 0$ in Fig. 5. By considering Fig. 5, the E_g bandgap energy values of the complexes **1**–**7** were obtained at 4.84, 5.51, 5.22, 5.54, 5.44, 5.55, and 5.33 eV, respectively (see Fig. 5). The theoretical energy gap obtained from FMO energies was calculated at 4.12, 3.07 for β spin, 4.06 for β spin, 1.87, 3.99 for α spin, 3.20 for β spin, and 3.06 for β spin for the complexes **1**–**7**, respectively. It can be said that these results are comparable with each other.

In this context, to determine the relationship among the physicochemical properties of the molecules, molecular chemical stability, and chemical reactivity, we examined energy gap results. To obtain FMO energy values of the complexes **1**–**7** in ethanol solvent, the HSE06/6-311G(d,p)/LanL2DZ level was used. It could be usually noted that the electron donating and electron withdrawing ability symbolize the HOMO and LUMO, respectively. It is seen in Fig. 4; the HOMO and LUMO energy values of the complexes **1**–**7** in ethanol solvent are calculated at the range from − 2.90 to − 6.94 eV for α spin and − 1.75 to − 2.85 eV for β spin, respectively. The χ, η, and S parameters, called electronegativity, chemical hardness, and softness, obtained from FMO energies are computed using equations given references therein [52, 62]. The χ, η, and S of the complexes **1**–**7** are found at the range of 4.96–2.41 eV for α spin, 2.06–0.49 eV for α spin, and 0.49–2.05 eV^{-1} for α spin, respectively. It could be concluded from these results that the complex **4** provided the efficient charge transfer and could be easily polarized.

The NBO calculations for the complexes **1**–**7** were applied using HSE06/6-311G(d,p)/LanL2DZ level. To survey inter- and intra-molecular bonding and interaction among bonds, as well as charge transfer or conjugative interaction in molecular system, NBO study was performed. The second-order perturbation approach [52, 63, 64] was applied

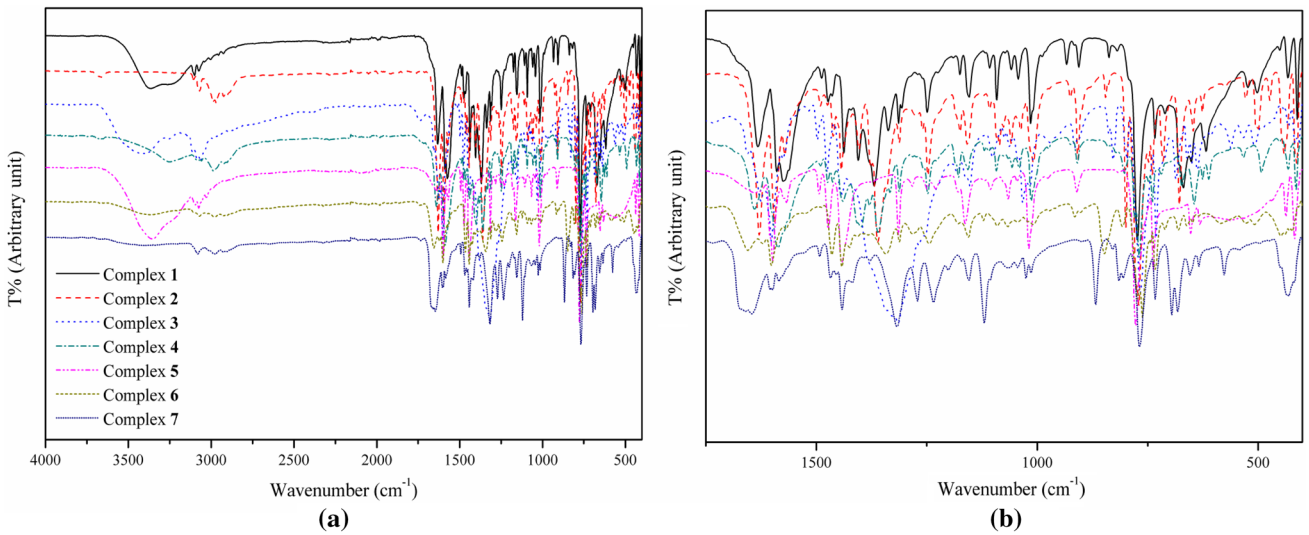

Fig. 2 FT-IR spectra of the complexes **1**–**7** at the range **a** 4000–400, **b** 1750–400

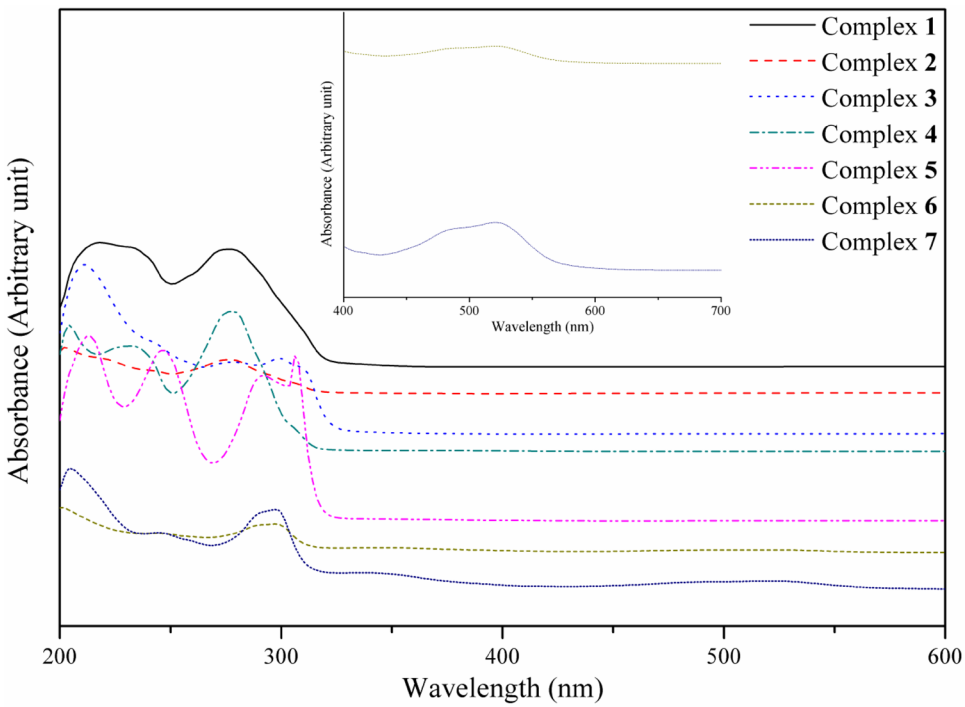

Fig. 3 UV–Vis spectra for the complexes **1**–**7**

to investigate the hyperconjugative interaction energies. Table S3 demonstrates the possible intensive interactions. The delocalization between lone-pair (n) orbitals of nitrogen/oxygen atom and anti-lone-pair (n*) orbitals of M(II) ion was clearly determined (see Table S3). This delocalization effect playing significant role on the coordination environments of the Hg(II), Co(II), Cu(II), Mn(II), Ni(II), and Fe(II) ions in the complexes **1**–**7** was appointed as $n \rightarrow n^*$ interactions. The coordination geometries were verified by these interactions of the complexes **1**–**7**. The $E^{(2)}$ values for the complexes **1**–**7** defined as the stabilization energy were found to be 178.48 and 0.44 kcal/mol range. The remarkable interaction energies of $LP(3)O \rightarrow \pi^*(C–O)$ showing interaction between the carbonyl group and the oxygen atom bound to the metal ion were obtained at the range of 78.27 and 30.57 kcal/mol. Moreover, Table S3 presents the stabilization interactions in 6-mpa and bpy ligands as well as hydrogen-bonding interactions for the complexes **1**, **2**, **5**–**7**.

In the research of relation between structure–activity and physicochemical properties of compounds containing

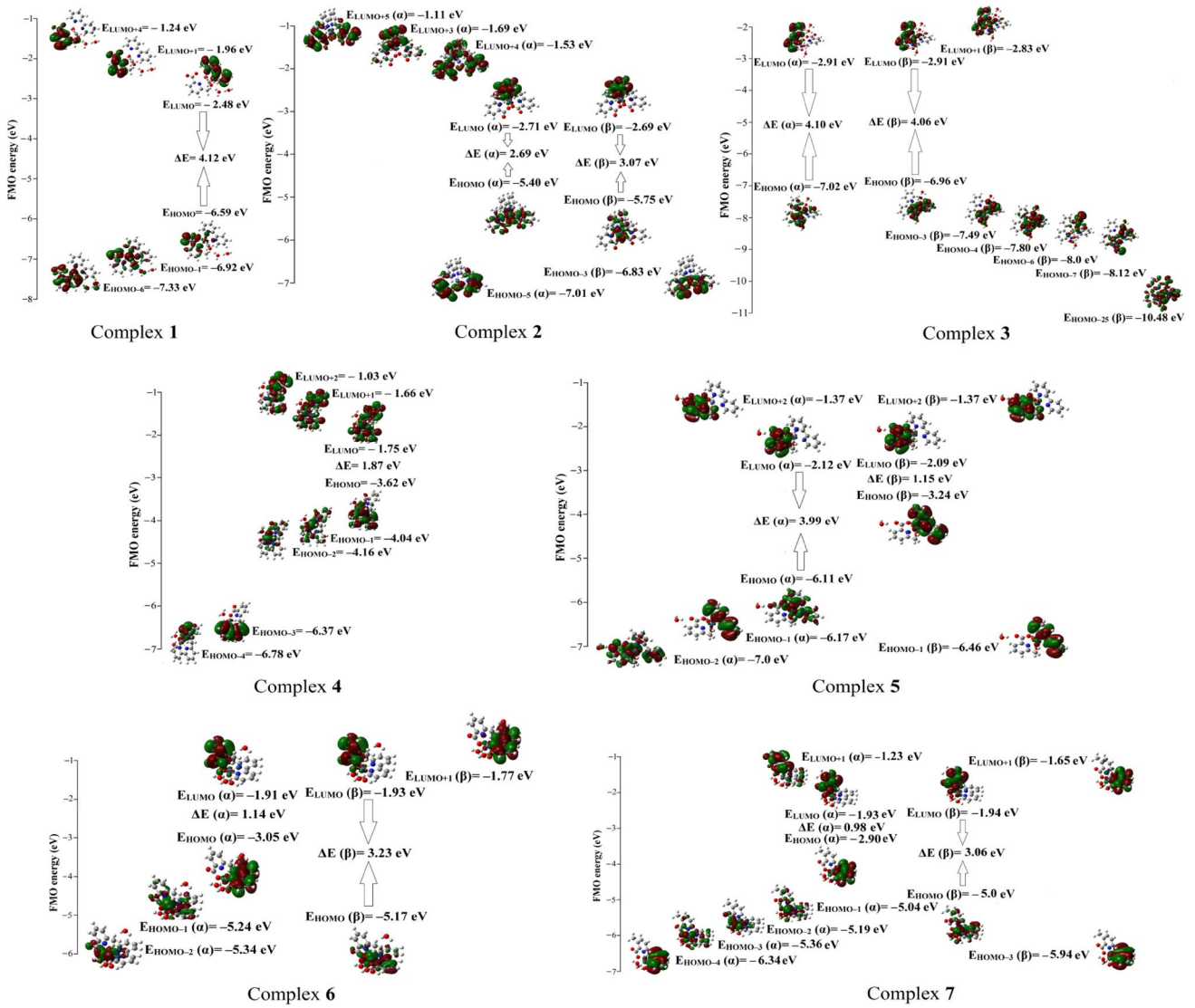

Fig. 4 Most active occupied and unoccupied molecular orbitals in electronic transition of the complexes **1**–**7** obtained by HSEh1PBE level in ethanol solvent

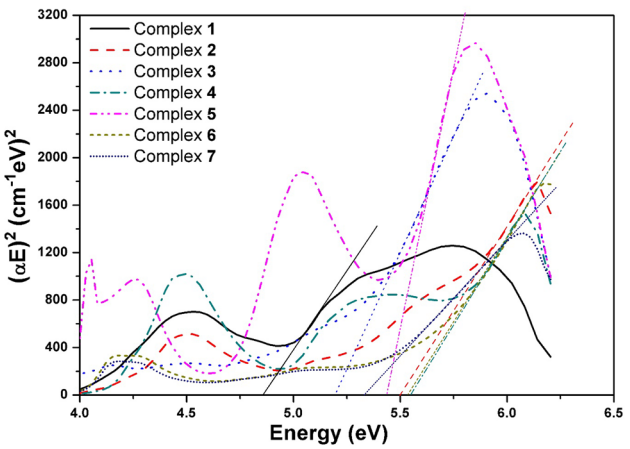

Fig. 5 Graphs of optical bandgap energy for the complexes **1**–**7**

biomolecules and drugs [65, 66], the MEP surface is remarkably used. The MEP describes molecular shape, size and ESP regions interconnecting color classification at the same time. Figure 6 depicts the MEP surfaces of complexes **1**–**7**. The MEP color code values between the deepest red and blue for the complexes **1**–**7** are range from − 9.900e−2 to 9.900e−2 a.u., − 9.645e−2 to 9.645e−2 a.u., − 7.936e−2 to 7.936e−2 a.u., − 8.171e−2 to 8.171e−2 a.u., − 7.383e−2 to 7.383e−2 a.u., − 7.134e−2 to 7.134e−2 a.u., and − 6.819e−2 to 6.819e−2 a.u., respectively. The negative regions represented by red color determining electrophilic reactivity are over the electronegative O atoms belonging the carboxylate groups and water ligands uncoordinated with M(II) ions. The positive regions surrounding H atoms connect to C described

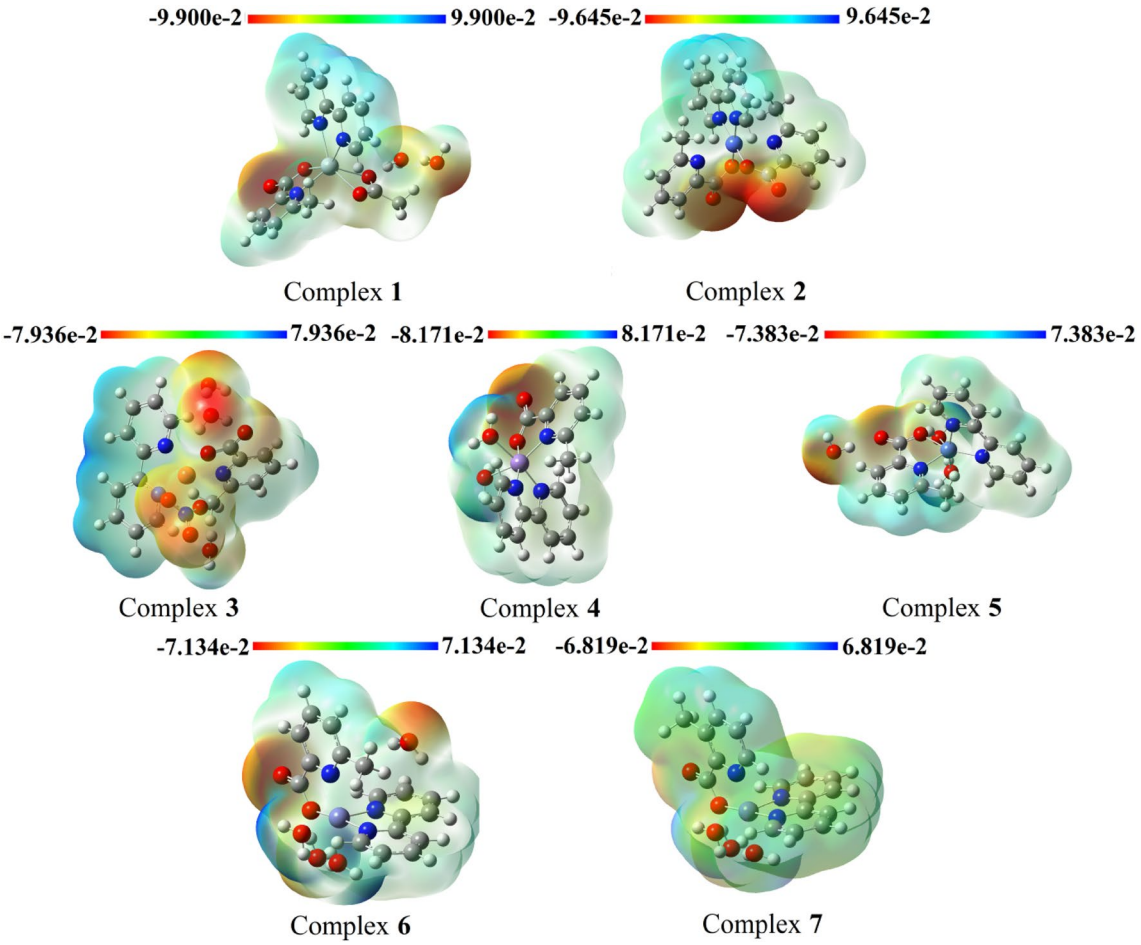

Fig. 6 Molecular electrostatic potential (MEP) surfaces for the complexes **1**–**7** obtained by HSEh1PBE level in gas phase

by blue color attributed to nucleophilic reactivity, as can be seen in Fig. 6.

Analysis of second-order and third-order nonlinear optical parameters

Recently, nonlinear optical (NLO) materials have been great attention with regard to new potential applications in the field of optical communication, optical switching, and dynamic image processing [67–69]. The development of device application for organic, inorganic, and organometallic NLO materials is possible with involving both theoretical and experimental studies in different fields, such as physics, engineering, etc. To understand the electronic polarization underlying the molecular NLO processes and establish of structure–property relationships, theoretical calculations provide an important contribution.

To investigate the LO and NLO parameters of the complexes **1**–**7** in gas phase and ethanol solvent, the HSE06 level was used (see Table S4). It could be said that all LO and NLO parameters of the complexes **1**–**7** show substantial difference/similarity owing to M(II) ions and theirs coordination environments. Table S4 displays that there is remarkable second-order β and third-order γ parameters for the complexes **2**, **4**, **5** due to d-orbital effect on the coordination geometry around M(II) ions. The α, $\Delta\alpha$, β, and γ parameters of the complexes **1**–**7** in gas phase and ethanol solvent were calculated using equations given references therein [52, 53, 69]. To compare LO and NLO parameters for molecular systems without experimental measurements, the results of *p*-nitroaniline (pNA), nitrobenzene [70–72] and urea [73], which are the prototypical compounds, were used. The β values of the complexes **1**–**7** in gas phase and ethanol solvent were found to be 62×10^{-30} to 4.7×10^{-30} esu and 268.5×10^{-30} to 5.4×10^{-30} esu, respectively. It is clear from Table S4 that the largest β value obtained for the complex **4** in gas phase and ethanol solvent is of 62×10^{-30} and 268.5×10^{-30} esu. These results demonstrate 476.92/6.74 and 2065.38/29.18 times higher than those of urea (0.130×10^{-30} esu)/pNA (9.2×10^{-30} esu). Similarly, the γ values for complex **4** in gas phase and ethanol solvent are obtained at 43.8×10^{-36} esu and 441.5×10^{-36} esu,

respectively. These values are about 2.92 and 29.43 times higher than that of pNA (15×10^{-36} esu). By evaluating the calculated β and γ parameters in gas phase and ethanol solvent, it could be said that complex **4** is a powerful indicator for microscopic second-order and third-order NLO property. The linear polarizability (α) values of the complexes **1**–**7** in mentioned solvents are computed at the range of 68.6×10^{-24} and 39.2×10^{-24} esu. All of the calculated α values for the complexes **1**–**7** are higher than that of pNA (17×10^{-24} esu). According to our previous results, all results are comparable for the same parameters [7, 52, 53]. It could be interpreted that the main reasons for the change in the NLO parameters of these complexes are the charge mobility in the complex, the change of substitute, and metals in coordination complexes. In these complex structures, although the delocalization effect of π-electrons, π-conjugation chain length, and charge transfer is the forefront, the other important change in the NLO parameters is the symmetry center around M(II) ions. In brief, in terms of our previous results which have performed for different metal complexes of 6-mpa, it can be said that second-order and third-order NLO parameters for the complex **4** are notable.

α-Glucosidase inhibition analysis

The α-glucosidase activity studies of the synthesized complexes (**1**–**7**) were fulfilled according to literature [7, 40]. Table 4 shows the IC_{50} values for α-glucosidase inhibitions. Their IC_{50} values against α-glucosidase were obtained at varying range of 0.184 µM and > 600 µM. Among these complexes, the complex **1** (IC_{50} = 0.184 µM) displayed the strongest inhibitor activity against α-glucosidase. This value is 4923.91-fold, 90.08-fold, and 69.02-fold higher than that of acarbose (IC_{50} = 906 µM) [74, 75], well known as α-glucosidase inhibitors, genistein (IC_{50} = 16.575 µM), used as a standard in this study, and resveratrol (IC_{50} = 12.70 µM) [76, 77], respectively.

Table 4 In vitro inhibition IC_{50} values (µM) of the complexes **1**–**7** for α-glucosidase

Compound	IC_{50} (µM)[a]
6-Methylpicolinic acid (6-MpaH)	Not active
2,2′-Bipiridil (bpy)	Not active
Complex **1** [Hg(6-mpa)(bpy)(OAc)]·$2H_2O$	0.184 ± 0.015
Complex **2** Co(6-mpa)$_2$(bpy)	> 600
Complex **3** [Cu(6-mpa)(bpy)(NO_3)]·$3H_2O$	688.94 ± 1.41
Complex **4** Mn(6-mpa)(bpy)(H_2O)$_2$	> 600
Complex **5** [Ni(6-mpa)(bpy)(H_2O)$_2$]·H_2O	> 600
Complex **6** [Fe(6-mpa)(bpy)(H_2O)$_2$]·$2H_2O$	97.33 ± 0.22
Complex **7** [Fe(3-mpa)(bpy)(H_2O)$_2$]·H_2O	724.25 ± 0.66
Genistein	16.575 ± 0.23
Acarbose[b]	906
Resveratrol[c]	12.70

[a]IC_{50} values represent the mean ± SEM of three parallel measurements ($p < 0.05$)

[b]From Refs. [74, 75]

[c]From Refs. [76, 77]

The following points could be concluded from Table 4 with regard to structure–activity relationship (SAR):

1. Among complexes with the same coordination (complexes **1**, **2**, **4**–**7**), complex **1** including Hg has the best inhibitor activity (IC_{50} = 0.184 µM). In other complexes **2**, **4**, **5**, changing metals have not showed a significant effect on α-glucosidase inhibition. By considering to these results, it could be considered that the atomic diameter of Hg metal is larger than the other Co, Mn, Ni, and Fe metals, and thus, Hg complex is more bulky than the other complexes. Furthermore, according to the results of molecular docking, complex **1** was found to have more van der Waals interactions with the amino acid residues in the active site of the enzyme. It is clear that the coordination environment and interactions with the enzyme active site directly affect alpha-glucosidase inhibition.
2. For complexes **2**, **4**, **5**, the changing metals and ligands around coordination do not exhibited any effect on activity results (IC_{50} = > 600 µM for complexes **2**, **4**, **5**), while these changes for complexes **6**, **7** are determined showing an effect in activity results (IC_{50} = 97.33 µM for complex **6** and IC_{50} = 724.25 µM for complex **7**).
3. The complex **3** has a distorted trigonal bipyramidal geometry, whereas the complexes **1**, **2**, **4**–**7** have a distorted octahedron geometry. This difference for complex **3** displays minor variation in enzyme activity result.
4. In comparison of α-glucosidase inhibition for the complexes **6** (IC_{50} = 97.33 µM) and **7** (IC_{50} = 724.25 µM), moving the methyl group from 6-position to 3-position at the mpa decreased almost 7.4-fold α-glucosidase inhibition. It is considered that the reason of this decrease is the steric effect of methyl group on carbonyl group.

To date, the IC_{50} values of various metal complexes of picolinate (pa) and its derivatives against α-glucosidase, such as Cu(pa)$_2$, Zn(pa)$_2$, VO(pa)$_2$ [30] and Zn(6mpa-ma)$_2$$SO_4$ [30] have been reported changing range 1.28 µM, 15.4 µM, > 1 mM, 7.5 µM for maltose and 9.6 µM for sucrose. Last decades, the studies on synthetic or natural α-glucosidase inhibitors have also increased significantly [10, 18] α-glucosidase inhibition values (IC_{50} values) reported that the previous studies were found at the range of 0.50 and > 200 µM. Furthermore, α-glucosidase inhibition values of our previously synthesized mixed-ligand (6-mpa and NCS/4(5)MeI) metal complexes were obtained at the

range of 2.910 μM and > 600 μM [7, 35]. In the present work, among the synthesized mixed-ligand (6-mpa and bpy) complexes of Hg(II), Co(II), Cu(II), Mn(II), Ni(II), and Fe(II) metals, the complex **1** has shown high inhibitory activity against α-glucosidase.

Considering X-ray crystallographic and molecular-docking studies on the inhibition mechanism of glucosidases, it is estimated that the hydrolysis can occur as a result of formation of anhydride moiety between the carbonyl of the complexes **1**–**7** and carboxylate group of the amino acid residues in the enzyme active site. Besides, it is detected that the interactions of hydrogen-bonding and van der Waals among synthesized complexes and amino acid residues effect on the α-glucosidase inhibition.

In vivo cytotoxic assay of the complex 1 was evaluated. The cytotoxic effect of the Hg(II) complex (complex **1**) was determined using the MTT assay on healthy cell. The IC_{50} value was calculated as 24.141 ± 1.039 μM, which is 131.20-fold less than IC_{50} value of 0.184 ± 0.015 μM for enzyme inhibition. According to this result, it can be assumed that the toxic effect of complex **1** on the healthy cell is negligible at concentrations exhibiting glucosidase inhibitory activity. In comparison of the previous studies above, it is obvious that complex **1** (IC_{50} = 0.184 μM) is the best α-glucosidase inhibitor.

Analysis of molecular docking

To demonstrate protein–ligand interactions between the synthesized complexes (**1**–**7**) and target protein [the template structure *S. cerevisiae* isomaltase (PDBID: 3A4A)], we performed the molecular-docking study using the iGEMDOCK program [49]. To provide more clearly evaluation of in vitro results, the results of electrostatic (E), hydrogen-bonding (H), and van der Waals (V) interactions for the protein–complex profiles were identified. Table S5 displays the estimated interactions and theirs energy values for the complexes **1**–**7**. The stabilization structures of the complexes **1**, **3**, **6**, **7** given in Fig. 7 show interacting of complex structures with amino acid residues through some hydrogen-bonding and van der

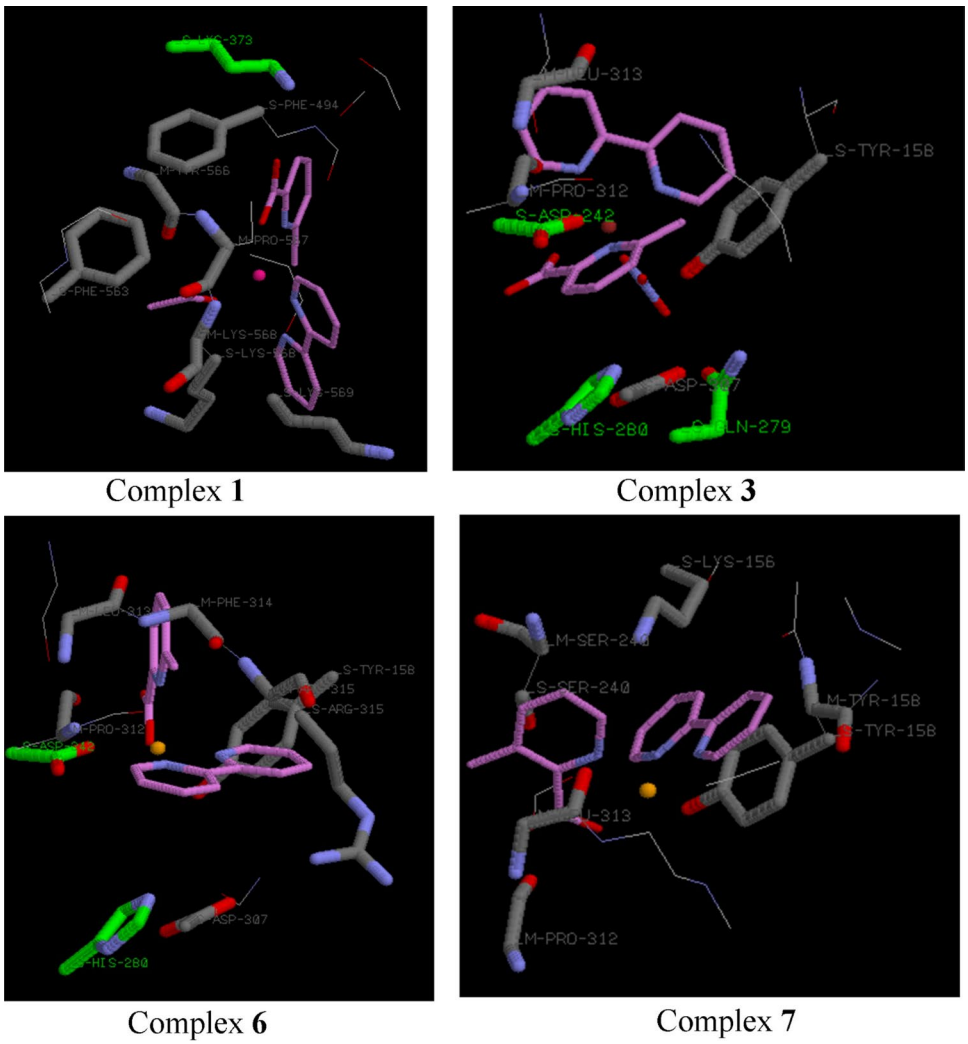

Fig. 7 3-D structures showing interactions between main/side chain amino acids and ligand of the complexes **1**, **3**, **6**, **7**

Waals interactions. It is clear that the energy values of V interactions forming between the same amino acid residues and non-coordinated parts of ligands around M(II) ions depend on ligand and metal type.

Complex **1** (0.184 ± 0.015 μM), which is the Hg metal ion complex, exhibited the most inhibitor activity among the complexes having bpy ligand substitution. According to docking results, total energy value of complex **1** calculated at − 93.0 kcal/mol displays that more interaction between the complex and amino acid residues. In the same or different amino acid residues interactions, the total hydrogen-bonding interaction energy values for complexes **1**–**7** were obtained at the range of − 3.5 and − 18.4 kcal/mol. In general, the H-bonding interactions for complexes **1**–**7** originate from the carbonyl oxygen atom of 6-mpa ligand or O atom of nitrate ligand with O^{δ}, N^{ξ} of same or different amino acid residues. In spite of emerging more H interactions for the complexes **2**, **3**, the α-glucosidase enzyme inhibition results (> 600 μM) were observed at lower level. For complex **6**, prominent H interaction obtained at − 8.1 kcal/mol energy value is determined between the S (side chain)-ASP242 O^{δ} (with 2.67 Å bond distance) and carbonyl oxygen atom of 6-mpa ligand. Likewise, major H interactions for the complexes **2**, **3** calculated at − 2.5 and 5.5 kcal/mol energy values are defined between the S-ASP242 O^{δ} (with 3.05 and 2.80 Å bond distance) and carbonyl oxygen atom belonging to 6-mpa ligand/nitrate ligand. In complexes **1**–**7**, even though complex **1** includes less H interactions with − 3.5 kcal/mol energy, it is more active than the other complexes **2**–**7**. We have also fulfilled ligand (6-mpa and bpy)-based docking study, It was observed the interactions between the amino acid residue and ligand the same as complex–protein interactions in different energy values. These energy differences can be explained as the reason for the change in their inhibition values.

In brief, the docking and in vitro results is remarkable scientific report for mixed-ligand (6-mpa and bpy) complex in use of complex **1** as novel drug candidate for DM II.

Conclusion

The complexes **1**–**7** {$[Hg(6\text{-mpa})_2(bpy)(OAc)]\cdot 2H_2O$, (**1**), $[Co(6\text{-mpa})_2(bpy)_2]$, (**2**), $[Cu(6\text{-mpa})(bpy)(NO_3)]\cdot 3H_2O$, (**3**), $[Mn(6\text{-mpa})(bpy)(H_2O)_2]$, (**4**), $[Ni(6\text{-mpa})(bpy)(H_2O)_2]\cdot H_2O$, (**5**), $[Fe(6\text{-mpa})(bpy)(H_2O)_2]\cdot 2H_2O$, (**6**), $[Fe(3\text{-mpa})(bpy)(H_2O)_2]\cdot H_2O$, (**7**)} as the potential α-glucosidase inhibitors were first synthesized and their structure characterizations were performed by XRD, LC–MS/MS, FT–IR, and UV–Vis spectra. The IC_{50} values of the synthesized complexes (**1**–**7**) for α-glucosidase inhibition were found to be between 0.184 and > 600 μM range. According to these results, complex **1**, which is a potential α-glucosidase inhibitor candidate, demonstrates the strongest inhibitor activity against α-glucosidase. Furthermore, to investigate the detailed structural, vibrational and electronic properties and to interpret to the corresponding experimental results, TD/DFT calculations with HSE06 method and 6-311G(d,p)/LanL2DZ basis set were carried out. Electronic spectra and theoretical results for the complexes **1**–**7** displayed that metal–ligand and ligand–ligand charge transfer were assigned as $n \rightarrow \pi^*$ and $\pi \rightarrow \pi^*$ transitions. The $d \rightarrow d$ (MMCT) and MLCT transitions for the complexes **2**–**7** were emerged as theoretical absorption peaks. It is clearly determined that NBO results confirm the coordination between LP electrons of the donor N/O atoms and M(II) ions in complexes **1**–**7**. It is clearly said that there is a well agreement between the theoretical and corresponding experimental results. According to the NLO results, it could be concluded that the complex **4** is a powerful indicator for microscopic second-order and third-order NLO property. Considering in vitro and docking studies, present paper is a remarkable scientific study of mixed-ligand complexes containing 6-mpa and bpy ligands that suggests the use of complex **1** as novel strong drug candidate for DM II.

Supplementary data Crystallographic data for the structural analysis has been deposited with the Cambridge Crystallographic Data Centre, CCDC Numbers: 1812523 (complex **1**) and 1857711 (complex **2**). Copies of this information may be obtained free of charge from the Director, CCDC, 12 Union Road, Cambridge CB2 1EZ, UK (fax: + 44-1223-336033; e-mail: deposit@ccdc.cam.ac.uk or http://www.ccdc.cam.ac.uk).

Acknowledgements This work was supported by the Scientific and Technological Research Council of Turkey (TÜBİTAK) (Project number: MFAG-117F235).

References

1. Cai CY, Rao L, Rao Y, Guo JX, Xiao ZZ, Cao JY, Huang ZS, Wang B (2017) Analogues of xanthones-Chalcones and bis-chalcones as alpha-glucosidase inhibitors and anti-diabetes candidates. Eur J Med Chem 130:51–59
2. Zhen J, Dai YJ, Villani T, Giurleo D, Simon JE, Wu QL (2017) Synthesis of novel flavonoid alkaloids as alpha-glucosidase inhibitors. Bioorg Med Chem 25(20):5355–5364
3. Ghani U (2015) Re-exploring promising a-glucosidase inhibitors for potential development into oral anti-diabetic drugs: finding needle in the haystack. Eur J Med Chem 103:133–162
4. Chaudhry F, Naureen S, Choudhry S, Huma R, Ashraf M, Al-Rashida M, Jahan B, Hyder Khan M, Iqbal F, Ali Munawar M, Ain Khan M (2018) Evaluation of alpha-glucosidase inhibiting potentials with docking calculations of synthesized arylidene-pyrazolones. Bioorg Chem 77:507–514
5. Sun H, Zhang YZ, Ding WN, Zhao X, Song XT, Wang D, Li YS, Han KL, Yang Y, Ma Y, Wang RL, Wang D, Yu P (2016)

Inhibitory activity evaluation and mechanistic studies of tetracyclic oxindole derivatives as alpha-glucosidase inhibitors. Eur J Med Chem 123:365–378
6. Barakat A, Islam MS, Al-Majid AM, Ghabbour HA, Yousuf S, Ashraf M, Shaikh NN, Choudhary MI, Khalil R, Ul-Haq Z (2016) Synthesis of pyrimidine-2,4,6-trione derivatives: anti-oxidant, anti-cancer, alpha-glucosidase, betaglucuronidase inhibition and their molecular docking studies. Bioorg Chem 68:72–79
7. Avcı D, Altürk S, Sönmez F, Tamer Ö, Başoğlu A, Atalay Y, Kurt BZ, Dege N (2018) Three novel Cu(II), Cd(II) and Cr(III) complexes of 6-methylpyridine-2-carboxylic acid with thiocyanate: synthesis, crystal structures, DFT calculations, molecular docking and α-glucosidase inhibition studies. Tetrahedron 74:7198–7208
8. Adisakwattana S, Charoenlertkul P, Yıbchok-Anun S (2009) α-Glucosidase inhibitory activity of cyanidin-3-galactoside and synergistic effect with acarbose. J Enzym Inhib Med Chem 24(1):65–69
9. Chiasson JL, Josse RG, Gomis R, Hanefeld M, Karasik A, Laakso M, STOP-NIDDM Trial Research Group (2002) Acarbose for the prevention of Type 2 diabetes, hypertension and cardiovascular disease in subjects with impaired glucose tolerance: facts and interpretations concerning the critical analysis of the STOP-NIDDM Trial data. Lancet 359:2072–2077
10. Santos CMM, Freitas M, Fernandes E (2018) A comprehensive review on xanthone derivatives as α-glucosidase inhibitors. Eur J Med Chem 157:1460–1479
11. Davies GJ, Mackenzie L, Varrot A, Dauter M, Brzozowski AM, Schülein M, Withers SG (1998) Snapshots along an enzymatic reaction coordinate: analysis of a retaining β-glycoside hydrolase. Biochemistry 37(34):11707–11713
12. Rye CS, Withers SG (2000) Glycosidase mechanisms. Curr Opin Chem Biol 4:573–580
13. McCarter JD, Withers SG (1996) 5-fluoro glycosides: a new class of mechanism-based inhibitors of both α- and β-glucosidases. J Am Chem Soc 118:241–242
14. Bian X, Fan X, Ke C, Luan Y, Zhao G, Zeng A (2013) Synthesis and α-glucosidase inhibitory activity evaluation of N-substituted aminomethyl-b-D-glucopyranosides. Bioorg Med Chem 21:5442–5450
15. Constable EC, Steel PJ (1989) *N*, *N′*-chelating biheteroaromatic ligands; a survey. Coord Chem Rev 93:205–223
16. Adams H, Bailey NA, Crane JD, Fenton DE, Latour JM, Williams JM (1990) Manganese (II) and iron (III) complexes of the tridentate ligands bis (benzimidazol-2-ylmethyl)-amine (L1) and -methylamine (L_2). Crystal structures of $[MnL_1 (CH_3CO_2)_2]$, $[FeL_2Cl_3]$, and $[Fe_2L_{12} (\mu\text{-}O)\{\mu\text{-}(CH3)_3 CCO_2\}_2][ClO_4]_2$. J Chem Soc Dalton Trans 5:1727–1735
17. Driessen WL, De Graaff RAG, Parlevliet FJ, Reedijk J, De Vos RM (1994) Transition metal compounds of the tridentate pyrazole substituted amine ligand bis (2-(3,5-dimethyl-1-pyrazolyl) ethyl) ethylamine (ddae). X-ray structures of $[Co(ddae)(NO_3)_2]$, $[Cu(ddae)(NO_3)(H_2O)](NO_3)$ and $[Cu(ddae)(Cl)_2]\cdot C_2H_5OH$. Inorg Chim Acta 216(1):43–49
18. Gollapalli M, Taha M, Javid MT, Almandil NB, Rahim F, Wadood A, Mosaddik A, Ibrahim M, Alqahtani MA, Bamarouf YA (2019) Synthesis of benzothiazole derivatives as a potent α-glucosidase inhibitor. Bioorg Chem 85:33–48
19. Demadis KD, Katarachia SD (2004) Metal-phosphonate chemistry: synthesis, crystal structure of calcium-amino tris-(methylene phosphonate) and inhibition of $CaCO_3$ crystal growth. Phosphorus Sulfur Silicon 179(3):627–648
20. Monot J, Petit M, Lane SM, Guisle I, Léger J, Tellier C, Talham DR, Bujoli B (2008) Towards zirconium phosphonate-based microarrays for probing DNA–protein interactions: critical influence of the location of the probe anchoring groups. J Am Chem Soc 130(19):6243–6251
21. Umeda J, Suzuki M, Kato M, Moriya M, Sakamoto W, Yogo T (2010) Proton conductive inorganic–organic hybrid membranes functionalized with phosphonic acid for polymer electrolyte fuel cell. J Power Sources 195(18):5882–5888
22. Saito BY, Takemoto J, Hutchinson B, Nakamoto K (1972) Infrared studies of coordination compounds containing low-oxidation-state metals I Tris(2,2′-bipyridine) and Tris(1, l0-phenanthroline) complexes. Inorg Chem 11(9):2003–2011
23. Amani V, Safari N, Khavasi HR (2007) Synthesis, characterization and crystal structure determination of iron(III) heteroligand complexes containing 2,20-bipyridine, 5,50-dimethyl-2,20-bipyridine and chloride, $[Fe(bipy)Cl_4][bipy\cdot H]$ and $[Fe(dmbipy)_2Cl_2][FeCl_4]$. Polyhedron 26:4257–4262
24. Mobin SM, Saini AK, Mishra V, Chaudhary A (2016) A series of new heteroleptic Hg(II) complexes: synthesis, crystal structures and photophysical properties. Polyhedron 110:131–141
25. Wang Y, Ma L, Li Z, Du Z, Liu Z, Qin J, Wang X, Huang Z, Gu L, Chen ASC (2004) Synergetic inhibition of metal ions and genistein on α-glucosidase. FEBS Lett 576:46–50
26. Shechter Y, Karlish SJD (1980) Insulin-like stimulation of glucose oxidation in rat adipocytes by vanadyl(IV) ions. Nature 284:556–558
27. Coulston L, Dandona P (1980) Insulin-like effect of zinc on adipocytes. Diabetes 29:665–667
28. Sorenson JRJ (1989) Copper complexes offer a physiological approach to treatment of chronic diseases. Prog Med Chem 26:437–568
29. Anderson RA, Cheng N, Bryden NA, Polansky MM, Cheng N, Chi J, Feng J (1997) Elevated intakes of supplemental chromium improve glucose and insulin variables in individuals with type 2 diabetes. Diabetes 46:1786–1791
30. Yasui H, Tamura A, Takino T, Sakurai H (2002) Structure-dependent metallokinetics of antidiabetic vanadyl-picolinate complexes in rats: studies on solution structure, insulinomimetic activity, and metallokinetics. J Inorg Biochem 91:327–338
31. Yasumatsu N, Yoshikawa Y, Adachi Y, Sakurai H (2007) Antidiabetic copper(II)-picolinate: impact of the first transition metal in the metallopicolinate complexes. Bioorg Med Chem 15:4917–4922
32. Yoshikawa Y, Ueda E, Kawabe K, Miyake H, Takino T, Sakurai H, Kojima Y (2002) Development of new insulinomimetic zinc(II) picolinate complexes with a $Zn(N_2O_2)$ coordination mode: structure characterization, in vitro, and in vivo studies. J Biol Inorg Chem 7:68–73 (**Erratum: JBIC J Biol Inorg Chem 7 (2002) 560–561**)
33. Yoshikawa Y, Hirata R, Yasui H, Sakurai H (2009) Alpha-glucosidase inhibitory effect of anti-diabetic metal ions and their complexes. Biochimie 91:1339–1341
34. Ueda E, Yoshikawa Y, Sakurai H, Kojima Y, Kajiwara NM (2005) In vitro α-glucosidase inhibitory effect of Zn(II) complex with 6-methyl-2-picolinmethylamide. Chem Pharm Bull 53(4):451–452
35. Avcı D, Altürk S, Sönmez F, Tamer Ö, Başoğlu A, Atalay Y, Kurt BZ, Dege N (2019) A novel series of M(II) complexes of 6-methylpyridine-2-carboxylic acid with 4(5) methylimidazole: synthesis, crystal structures, α-glucosidase activity, density functional theory calculations and molecular docking. Appl Organometal Chem 33:e4935
36. Sheldrick GM (2015) SHELXT—integrated space-group and crystal-structure determination. Acta Crystallogr A71:3–8
37. Macrae CF, Edgington PR, McCabe P, Pidcock E, Shields GP, Taylor R, Towler M, van de Streek J (2006) Mercury visualization and analysis of crystal structures. J Appl Crystallogr 39:453–457
38. Spek AL (2009) Structure validation in chemical crystallography. Acta Crystallogr D65:148–155

39. Sun H, Ding WN, Song XT, Wang D, Chen MZ, Wang KL, Zhang YZ, Yuan P, Ma Y, Wang RL, Dodd RH, Zhang YM, Lu K, Yu P (2017) Bioorg Med Chem Lett 27(15):3226–3230
40. Avcı D, Altürk S, Sönmez F, Tamer Ö, Başoğlu A, Atalay Y, Kurt BZ, Öztürk D, Dege N (2019) A new dinuclear copper (II) complex of 2,5-furandicarboxyclic acid with 4(5)-methylimidazole as a high potential α-glucosidase inhibitor: synthesis, crystal structure, cytotoxicity study, and TD/DFT calculations. Appl Organomet Chem 33:e4725
41. Frisch MJ, Trucks GW, Schlegel HB, Scuseria GE, Robb MA, Cheeseman JR, Scalmani G, Barone V, Mennucci B, Petersson GA, Nakatsuji H, Caricato M, Li X, Hratchian HP, Izmaylov AF, Bloino J, Zheng G, Sonnenberg JL, Hada M, Ehara M, Toyota K, Fukuda R, Hasegawa J, Ishida M, Nakajima T, Honda Y, Kitao O, Nakai H, Vreven T, Montgomery JA Jr, Peralta JE, Ogliaro F, Bearpark M, Heyd JJ, Brothers E, Kudin KN, Staroverov VN, Kobayashi R, Normand J, Raghavachari K, Rendell A, Burant JC, Iyengar SS, Tomasi J, Cossi M, Rega N, Millam JM, Klene M, Knox JE, Cross JB, Bakken V, Adamo C, Jaramillo J, Gomperts R, Stratmann RE, Yazyev O, Austin AJ, Cammi R, Pomelli C, Ochterski JW, Martin RL, Morokuma K, Zakrzewski VG, Voth GA, Salvador P, Dannenberg JJ, Dapprich S, Daniels AD, Farkas O, Foresman JB, Ortiz JV, Cioslowski J, Fox DJ (2013) Gaussian 09, Revision D.01. Gaussian, Inc., Wallingford
42. Dennington R, Keith T, Millam J (2009) GaussView, Version 5. Semichem Inc., Shawnee Mission KS
43. Heyd J, Scuseria GE (2004) Efficient hybrid density functional calculations in solids: assessment of the Heyd–Scuseria–Ernzerhof screened Coulomb hybrid functional. J Chem Phys 121:1187–1192
44. Krukau AV, Vydrov OA, Izmaylov AF, Scuseria GE (2006) Influence of the exchange screening parameter on the performance of screened hybrid functionals. J Chem Phys 125:224106
45. Frisch MJ, Pople JA, Binkley JS (1984) Self-consistent molecular orbital methods 25. Supplementary functions for Gaussian basis set. J Chem Phys 80:3265–3269
46. Hay PJ, Wadt WR (1985) Ab initio effective core potentials for molecular calculations. Potentials for the transition metal atoms Sc to Hg. J Chem Phys 82:270–283
47. Runge E, Gross EKU (1984) Density-functional theory for time-dependent systems. Phys Rev Lett 52:997–1000
48. Miertus S, Scrocco E, Tomasi J (1981) Electrostatic interaction of a solute with a continuum. A direct utilizaion of Ab initiomolecular potentials for the prevision of solvent effects. J Chem Phys 55:117–129
49. Yang J-M, Chen C-C (2004) GEMDOCK: a generic evolutionary method for molecular docking. Proteins 55:288–304
50. Glendening ED, Reed AE, Carpenter JE, Weinhold F (1998) NBO Version3.1, TCI. University of Wisconsin, Madison
51. Kukovec B-M, Popović Z, Kozlevčar B, Jagličić Z (2008) 3D supramolecular architectures of copper(II) complexes with 6-methylpicolinic and 6-bromopicolinic acid: synthesis, spectroscopic, thermal and magnetic properties. Polyhedron 27:3631–3638
52. Altürk S, Avcı D, Başoğlu A, Tamer Ö, Atalay Y, Dege N (2018) Copper(II) complex with 6-methylpyridine-2-carboxyclic acid: experimental and computational study on the XRD, FT-IR and UV–Vis spectra, refractive index, band gap and NLO parameters. Spectrochim Acta Part A Mol Biomol Spectrosc 190:220–230
53. Altürk S, Avcı D, Tamer Ö, Atalay Y, Şahin O (2016) A cobalt(II) complex with 6-methylpicolinate: synthesis, characterization, second- and third-order nonlinear optical properties, and DFT calculations. J Phys Chem Solids 98:71–80
54. Kukovec B-M, Vaz PD, Popović Z, Calhorda MJ, Furić K, Pavlović G, Linarić MR (2008) Pseudopolymorphism in nickel(II) complexes with 6-methylpicolinic acid. Synthesis, structural, spectroscopic, thermal and DFT study. Cryst Growth Des 8:3465–3473
55. Scott AP, Radom L (1996) Harmonic vibrational frequencies: an evaluation of Hartree–Fock, Møller–Plesset, quadratic configuration interaction, density functional theory, and Semiempirical scale factors. J Phys Chem 100:16502–16513
56. Varsanyi G (1973) Assignments for vibrational spectra of seven hundred benzene derivatives. Academic Kiaclo, Budapest
57. Pons J, March R, Rius J, Ros J (2004) Zinc complexes of 6-methyl-2-pyridinecarboxylic acid. Crystal structure of $[Zn(MeC_5H_3NCOO)_2(H_2O)]\cdot H_2O$. Inorg Chim Acta 357:3789–3792
58. Alizadeh R, Amani V (2016) Syntheses, crystal structures, and photoluminescence of three cadmium(II) coordination complexes based on bipyridine ligands with different positioned methyl substituents. Inorg Chim Acta 443:151–159
59. Belicchi-Ferrari M, Bisceglie F, Cavalieri C, Pelosi G, Tarasconi P (2007) Bis(triphenylphosphine)4-fluorobenzaldehyde thiosemicarbazone copper(I): forcing chelation through oxoanions. Polyhedron 26:3774–3782
60. Gorelsky SI (2010) SWizard Program Revision 4.5. University of Ottawa, Ottawa. http://www.sg.chem.net/
61. Şişman İ, Başoğlu A (2016) Effect of Se content on the structural, morphological and optical properties of $Bi_2Te_{3-y}Se_y$ thin films electrodeposited by under potential deposition technique. Mater Sci Semicond Process 54:57–64
62. Yang W, Parr RG (1985) Hardness, softness, and the fukui function in the electronic theory of metals and catalysis. Proc Natl Acad Sci USA 82:6723–6726
63. Reed AE, Weinhold F (1983) Natural bond orbital analysis of near-Hartree–Fock water dimer. J Chem Phys 78:4066–4073
64. Foster JP, Weinhold F (1980) Natural hybrid orbitals. J Am Chem Soc 102:7211–7218
65. Sponer J, Hobza P (1996) DNA base amino groups and their role in molecular interactions: ab initio and preliminary density functional theory calculations. Int J Quantum Chem 57:959–970
66. Gadre SR, Shrivastava IH (1991) Shapes and sizes of molecular anions via topographical analysis of electrostatic potential. J Chem Phys 94:4384–4390
67. Chemla DS, Zysss J (1987) Nonlinear optical properties of organic molecules and crystals. Academic Press, Orlando
68. Kamada K, Ueda M, Nagao H, Tawa K, Sugino T, Shmizu Y, Ohta K (2000) Molecular design for organic nonlinear optics: polarizability and hyperpolarizabilities of furan homologues investigated by ab initio molecular orbital method. J Phys Chem A 104:4723–4734
69. Pierce BM (1989) A theoretical analysis of third-order nonlinear optical properties of linear polyenes and benzene. J Chem Phys 91:791–811
70. Cheng L-T, Tam W, Stevenson SH, Meredith GR, Rikken G, Marder SR (1991) Experimental investigations of organic molecular nonlinear optical polarizabilities. 1. Methods and results on benzene and stilbene derivatives. J Phys Chem 95:10631–10643
71. Kaatz P, Donley EA, Shelton DP (1998) A comparison of molecular hyperpolarizabilities from gas and liquid phase measurements. J Chem Phys 108:849–856
72. Stahelin M, Burland DM, Rice JE (1992) Solvent dependence of the second order hyperpolarizability in *p*-nitroaniline. Chem Phys Lett 191:245–250
73. Adant C, Dupuis M, Bredas JL (2004) Ab initio study of the nonlinear optical properties of urea: electron correlation and dispersion effects. Int J Quantum Chem 56:497–507
74. Taha M, Hadiani Ismail N, Lalani S, Qaiser Fatmi M, Atia-tul-Wahab, Siddiqui S, Khan KM, Imran S, Iqbal Choudhary M (2015) Synthesis of novel inhibitors of α-glucosidase based on

the benzothiazole skeleton containing benzohydrazide moiety and their molecular docking studies. Eur J Med Chem 92:387–400
75. Taha M, Hadiani Ismail N, Syukri Baharudin M, Lalani S, Mehboob S, Khan KM, Yousuf S, Siddiqui S, Rahim F, Choudhary MI (2015) Synthesis crystal structure of 2-methoxybenzoylhydrazones and evaluation of their α-glucosidase and urease inhibition potential. Med Chem Res 24:1310–1324
76. Zheng J-W, Ma L (2015) Silver(I) complexes of 2,4-dihydroxybenzaldehyde–amino acid Schiff bases-Novel noncompetitive α-glucosidase inhibitors. Bioorg Med Chem Lett 25:2156–2161
77. Zheng J-W, Ma L (2016) Metal complexes of anthranilic acid derivatives: a new class of non-competitive α-glucosidase inhibitors. Chin Chem Lett 27:627–630